Synthesis and Characterization of Iron Oxide Nanoparticles Using *Syzygium aromaticum* Extracts and their Activity on Organic Dye and Phytopathogen

In present study, biosynthesis of iron oxide nanoparticles using clove (*Syzygium aromaticum*) extracts was performed and characterized. The activity of the biosynthesized iron oxide nanoparticles was evaluated against phytopathogen (*Colletotrichum falcatum*) and the result showed that the biogenic nanoparticles produced antifungal activity on the test organism. The photocatalytic activity of the present study revealed a rapid and efficient degradation of methylene blue within 0.5 h.

Keywords: Iron oxide, Nanoparticles, Biosynthesis. Antifungal activity.

INTRODUCTION

In sensor development, the synthesized metal nanoparticles can be integrated with a living (bio) molecules for the enhancement of the sensor or it can be used solely for the fabrication of sensor for an analyte detection [1]. It can also take part in determination of drug residues in food that includes antibiotics, monitoring of glucose in diabetes patients as well as biosensor for the detection of pathogens [1,2]. Nanoparticles offer an enhanced detection limit for the detection of pathogens in plant such as viruses and fungi. It can also be used as biomarker for the rapid diagnostic/detection of plant diseases such as fungi, phytobacteria and viruses as well [2].

Some metal oxide nanoparticles have gained much consideration due to their potential role and efficacy in different areas which includes pharmacy, biomedicine, material science, *etc*. [3]. Silver nanoparticles contain antimicrobial properties [4-6] and can be used for ecofriendly pesticides safely [7,8]. Likewise, zinc oxide nanoparticles have shown that it could inhibit microorganisms such as fungi and bacteria [9,10]. However, the mode of action of the mechanisms of inhibition of zinc oxide nanoparticles for molecular process is still under investigation [9]. Iron oxide nanoparticles received more attention, since it has some unique properties such as super-paramagnetsim, multifunctional properties, large surface area, as well as surface-to-volume ratio [11]. The synthesis of iron oxide nanoparticles for nano-therapiests is an important requirement in biomedical activities [12,13].

Recently, intensive research attracts more attention in the synthesis of nanoparticles with uniform particle size due to its fundamental interest in the field of science as well as technological significance [14]. As the result of reducing their size, nanoparticles show unique properties. Mostly, iron oxide and ferrite attract increasing interest due to their significance in the field of nanotechnology of storage information, catalyst and other materials [15]. In addition to other features, for instance, magnetic iron oxides nanoparticles harbour important features such as biocompatibility; physico-chemical stability as well as relatively low toxicity [16], hence can be used for a wide applications including sensor and some other usage.

Cloves also play an important role in traditional medicine considered the main bioactive components found in clove. It has large concentrations of phenolic acid, garlic acid, flavonoids, *etc*. [17]. It has been reported that clove (*Syzygium aromaticum*) has some properties such antimicrobial (bacterial, fungal and viral) properties [18]. Clove (*Syzygium aromaticum*) has some properties such antimicrobial properties and ease of processing for various applications [19]. In this work, biosynthesis of iron

were oxide nanoparticles using clove (*S. aromaticum*) extracts was carried out and characterized. Antifungal activity of the biogenic nanoparticles was evaluated and the photocatalytic acitivity of these nanoparticles revealed a fast and efficient degradation of organic dye (methylene blue) within short time compared to some earlier reported methods.

EXPERIMENTAL

All the chemicals and reagents used in this study were all of analytical grade and the media was purchased from Himedia India.

Synthesis of iron oxide nanoparticles using plant material

Extraction of plant materials: The plant material (clove) *S. aromaticum* flower bud was extracted using the following method. Briefly, the dried clove buds purchased from the local market were washed with double distilled water and dried. It was then ground in to a fine powder. To extract the bioactive components of the plant materials, 1 g of fine powder of plant material was added in to 50 mL double distilled water and heated for 2 min. Then allowed to cool at room temperature and filtered using a Whatman filter paper. To obtain a pure or clear plant extracts, the filtered solution was also centrifuged at 12,000 rpm for 15 min and then stored at 20 ºC for further use.

write the temperature

Size of filter?

Biosynthesis of iron oxide nanoparticles: The biosynthesis of iron oxide nanoparticle was carried out by some modifications of the earlier reported methods [18,20,21]. Briefly, 1 mM of ferric chloride solution was added in to the plant extract, the reaction mixture was allowed for 1 h. After that the colour of the reaction mixture changed from transparent to dark, which confirmed the synthesis of iron oxide nanoparticles. The reaction mixture was then centrifuged at 12,000 rpm for 15 min and the sediments were washed three times with double distilled water followed by one wash with ethanol, dried and collected as an iron oxide nanoparticles.

the volume of plant extract

Write the incubation temperature

Write full name.

The biogenic iron oxide nanoparticles were characterized by FTIR, UV-visible, TGA, field emission scanning electron microscopy (FESEM), energy dispersive spectroscopy, DLS and zeta potential, *etc*. The dynamic light scattering (DLS) and zeta potential measurements were conducted using zeta sizer (Nano ZS, Malvern instruments UK). The sample was prepared by diluting the required amount of sample in double distilled water after sonicated for 20 min. A sample solution was then taken and put in a glass or plastic cuvette, after which the cuvette was placed in the cell holder and scanned. A temperature of 25 ºC was maintained in all the samples measurements.

Sample collection: A survey was conducted in sugarcane-growing areas and diseased samples were identified in the fields, and collected from the symptomatic canes showing red rots infected symptom and then transported to the laboratory for further use. To avoid contamination during the sample and media preparations, all the apparatus/materials used in this work were sterilized with autoclave at 121 ºC for 15 min.

Media preparation: All the media used in this research were prepared and sterilized according to the manufacturers' instructions.

Isolation and identification of *Colletotrichum falcatum*: *Colletotrichum falcatum* was isolated and identified according to the procedure described earlier [22,23]. The collected infected samples of the sugarcanes were split and opened using a sterilized knife and the reddish-tissue as well as white transverse band were observed. Tissue segment method was used for the isolation of the red rot pathogen (*C. falcatum*) as described previously. In this, the infected tissue was cut in to small pieces (2-5 mm) and then surface sterilized using 1% sodium hypochlorite for 1 min and then immersed in 70% ethanol for 1 min, respectively. Moreover, rinsed with distilled water and then dried on a sterilized tissue paper. After that, the samples were then inoculated aseptically on potato dextrose agar (PDA) and incubated at 28 ºC for 7 days [24]. The obtained mixed growth was then sub-cultured on a fresh media to obtain a pure culture. All the isolates were purified and identified *via* single spore technique as described by Pandey & Shukla [22]. When the fungus shows a sporulation, the spore were then picked up using a sterilized wire loop and then streaked on the surface of the medium. After overnight inoculating at 29 ± 2 ºC, the germinated single spores were picked using sterilized needle and transferred to another fresh medium. The cultures obtained were maintained at 4 ºC for further use. To obey the Koch's rule, the pathogenicity of the isolated fungus was tested using a plug method [24]. This was conducted by taking a small suspension of the fungal spore (1 mL), bored a hole in the sugarcane stem and then injected the spores and covered with cotton wool and allowed for some days. The morphological appearance of the colony such as colour of the colony, margin of the colony, topography and substrate colour were observed. Microscopic examinations were also used for the spore colour, as well as shape of the conidia. All the experiments were carried out in triplicate

Antifungal activity assay: In this study, to check the antifungal activity of the biogenic iron oxide nanoparticles, agar well diffusion method was used as reported earlier [25] with some modification. Briefly, a fungal cultures of 7-8 days old days grown on potato dextrose agar (PDA) were used. A 0.1 mL inoculum of the test organism (fungal pathogen) inoculated in to 20 mL molten saboured dextrose agar medium (SDA) in a tube culture followed by homogenization and then poured in to sterilized petri plates and allowed to solidified. Wells were then bored on the solidified agar plate using a cork borer. Various concentrations of the synthesized nanoparticles of 0.1, 0.2 and 0.3 mg/mL were prepared and then added in to the respective bored wells. A standard antifungal of hexahit (0.1 mg/mL) was used as positive control while distilled as negative control, respectively. The plates were sealed and incubated at 25 ± 2 ºC for 5-7 days. After incubation, the zones of inhibition observed were measured and compared with positive and negative control recorded as well.

Photocatalytic activity: The study of the photocatalytic activity of biosynthesized iron oxide nanoparticles was conducted *via* the measurement of dye methylene blue degradation in the presence of Fe-oxide nanoparticles by some modification of earlier reported method [26,27]. In brief, 0.1 g catalyst was added in 100 mL of methylene blue dye solution (50 mg/L).

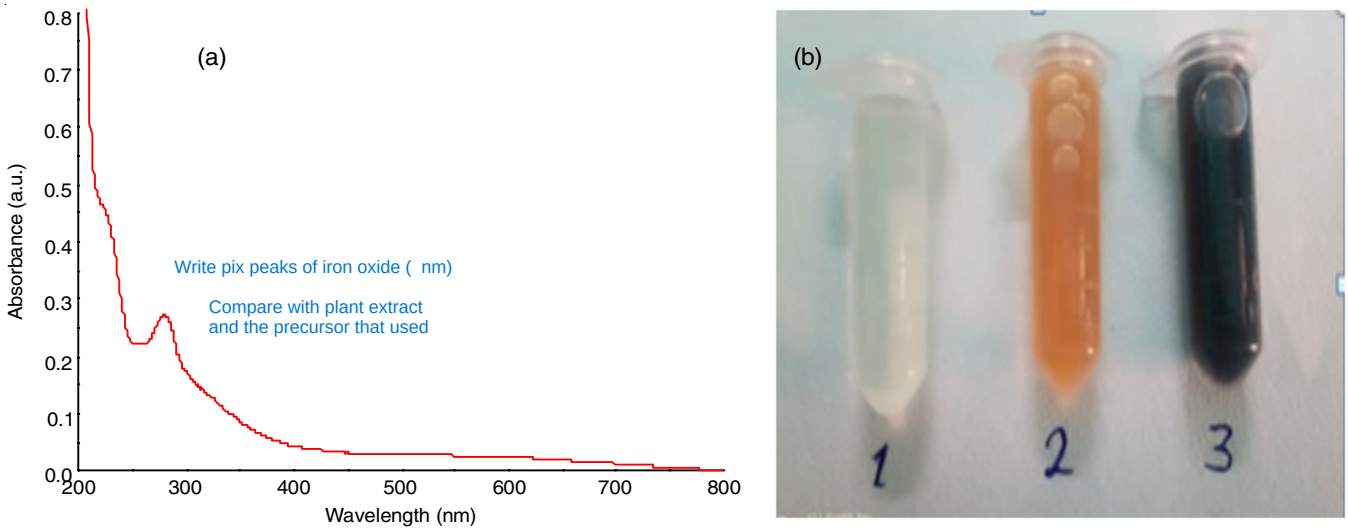

Fig. 1. (a) UV-Vis of the biogenic nanoparticles and (b) change of colour from transparent to dark

This was done by stirring for about 20 min in dark place prior to sunlight exposure. Same procedure was used for control but without adding the catalyst (synthesized nano-particles). The mixture/suspension was then taken to sunlight under constant magnetic stirring. The mixture/suspension was also taken for UV-vis measurements at regular interval of time. The percentage degradation was calculated by:

$$\text{Degradation } (\%) = \frac{C_o - C_t}{C_o} \times 100$$

where C_o and C_t represents initial and final concentration at which the degradation occurred, respectively.

RESULTS AND DISCUSSION

Biosynthesis of iron oxide nanoparticles: The biosynthesis of iron oxide nanoparticles were conducted using a ferric chloride solution added in to the plant extracts (clove). The changed of colour of the reaction mixture from transparent to dark confirmed the synthesis of iron oxide nanoparticles as shown in Fig. 1b, this is in line with the results obtained by Mishra *et al*. [24].

UV-Vis spectroscopy: UV-visible absorption spectrum is shown in Fig. 1a, the absorption peak observed at 280 nm confirmed the synthesis of iron oxide nanoparticles as this result is closely related to the result obtained previously [20,22].

FTIR analysis: FTIR was carried out within the range of 4000-500 cm^{-1}. The strong absorption peak at 3342 cm^{-1} was due to vibrational of O-H stretching bond of alcohols or phenols present in the sample which was relatively closed to reported results [18]. The absorption peak at 2992 cm^{-1} confirmed the O-H stretching bond of phenols (Fig. 2). Peak at 1712 cm^{-1} is due to C=O stretching bond of carboxylic acids, while the peak at 1593 cm^{-1} of N-H bending bond of amine. Peak observed at 1346 cm^{-1} of O-H bending bond phenol. A strong and broad peak of 1030 cm^{-1} is due to vibrational CO-O-CO bond. Peaks at 871 cm^{-1} and 758 cm^{-1} are due to C-H bending strong bond present in the sample and also within the range relatively closed to the existence of Fe-O, respectively [28]. Finally, the presence

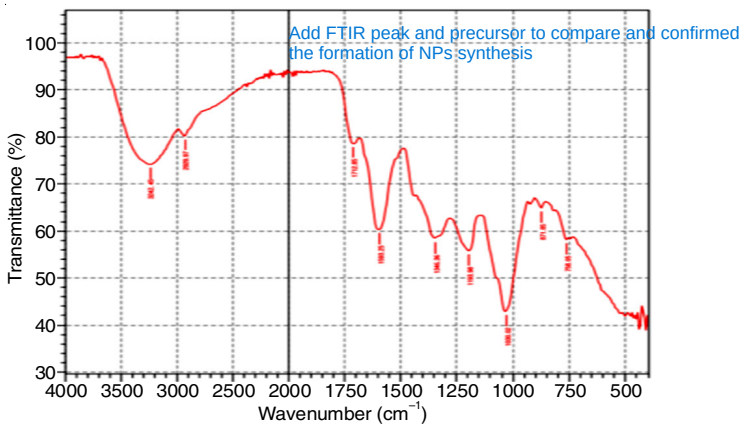

Fig. 2. FTIR bands (cm^{-1}) of biosynthesized iron oxide nanoparticles

of O-H (phenol) and N-H amides group (proteins) are responsible in reducing the precursor compound in to iron oxide nanoparticles [29].

Zeta potential: Dynamic light scattering (DLS) and zeta potential were investigated. To obtain the particles size distribution in the hydrodynamic medium, dynamic light scattering was investigated as shown in Fig. 3a. From the results obtained, it shows that the average diameters of the particles size are 358.3, 369.8, 370.9 with mean value of 366 having standard deviation of ± 6.6. While the zeta potential (Fig. 3b) has a mean value of 30 mV with standard deviation of ± 1.5 confirmed the stability of the biogenic nanoparticles, since nanoparticles with zeta potential plus or -30 mV shows a good stability and iron oxide nanoparticles properties depend largely upon particle size [18]. It also reported that nanoparticles ± 25 mV indicates a high stability of the nanoparticles [30].

Morphology: To obtain the surface morphology of the synthesized iron oxide nanoparticles, field emission scanning electron microscopy (JEOL JSM-7610 FPlus) was conducted. It can be seen that the synthesized nanoparticles shows a spherical shapes (Fig. 4a), this is similar to one of the findings of Naz *et al.* [29] and also relatively similar to Mirza *et al.* [31] and the size of the particles ranges from 5 to 50 nm.

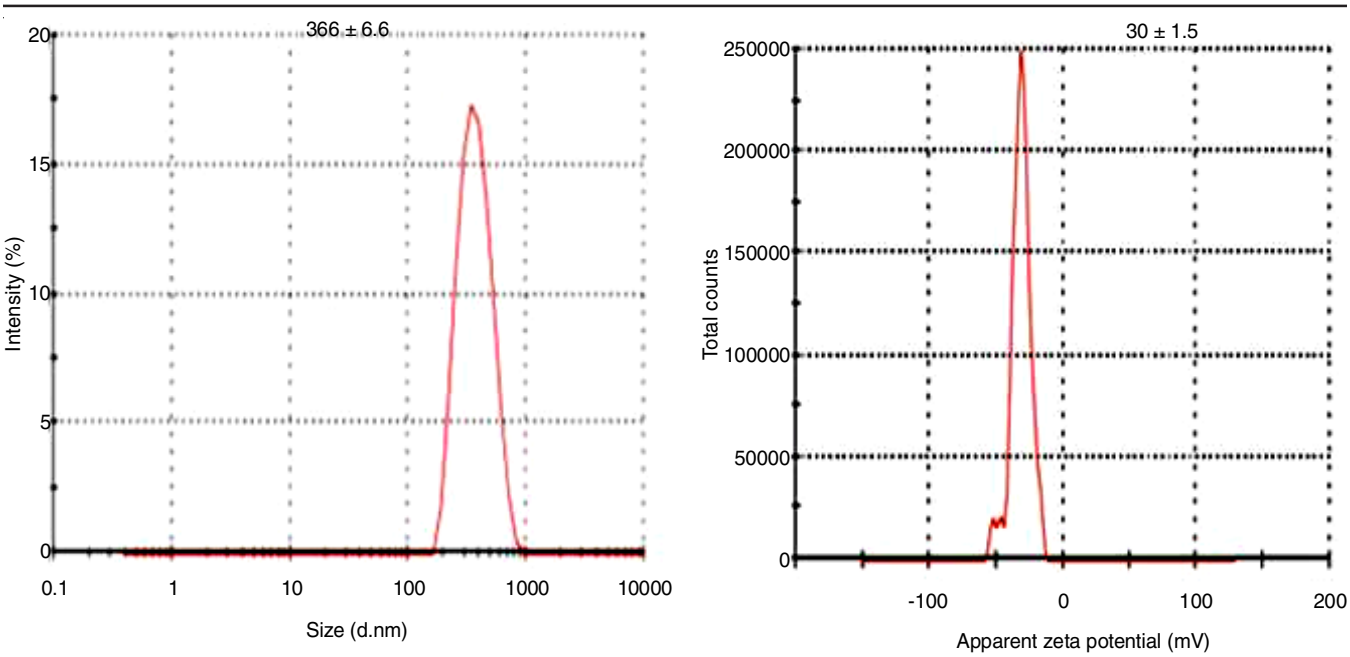

Fig. 3. (a) Dynamic light scattering and (b) zeta potential of biosynthesized iron oxide nanoparticles

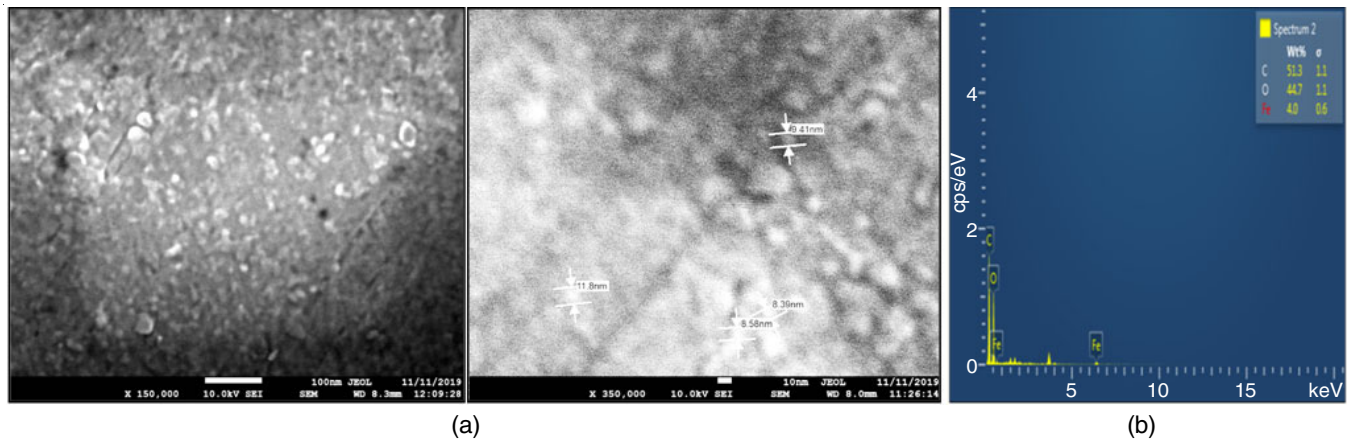

Fig. 4. (a) FESEM showing the morphology of the biogenic nanoparticles and (b) EDX of the biosynthesized nanoparticles

EDS analysis: Energy dispersive spectroscopy (EDS) as shown in Fig. 4b was carried out to screen the elements present in the biogenic iron oxide nanoparticles and confirmed that iron and oxygen elements are the constituents of the biogenic nanoparticles, while the presence of carbon element may be attributed due to the clove extract biomolecule in the sample [21].

Thermal studies: Thermal analysis of the synthesized iron oxide nanoparticles was investigated from 25 to 994 ºC and heated at 10 ºC/min. From the result obtained in the TGA plot, it has shown that the mass of the synthesized nanoparticles gradually decreases as the temperature increases (Fig. 5). However, it was found that the synthesized biogenic nanoparticle is stable up to 990 ºC. The reduced in weight loss had happened due to the thermal decomposition of biomolecules compound coated nanoparticles and the physically absorbed water [28].

Isolation and identification of *C. falcatum*: Red rot (cancer of sugarcane) caused by *C. falcatum* Went is the most devastating sugarcane problem (*Saccharum officinarum L.*)

Could you please add the pictures of Petri dishes.

which causes the serious losses of yields [24]. From the results obtained as shown in Table-1, it can be seen that the colour of the colony shows a white and white-grey appearance while the color of the substrate has shown a white; which is relatively similar with the results obtained by Pandey & Shukla [22]. In addition, the substrate colour shows a white in all the isolates with smooth and irregular margin as well as fluffy ans fluffy raised topography. The fungus also produced a spores, where are in agreement with the earlier obtained results [22,23].

Antifungal activity assay: The antifungal activity of the synthesized iron oxide nanoparticle was evaluated and the zones of inhibition were obtained in different concentrations of nanoparticles (0.1, 0.2 and 0.3 mg/mL) and were found to be 17.3, 19.2 and 21.4 mm, respectively. It was then compared with zone of inhibition recorded with positive control (26.3 mm) as well. No significance inhibition zone was observed in the negative control. The mechanisms of these inhibition was attributed to the bioactive components found in the nanoparticles as well as possession of small size and large surface

Add the pictures of antifungal activity assay to see the inhibition zone.

Prove your results of this table by adding pictures.

TABLE-1
CULTURAL AND MORPHOLOGICAL CHARACTERISTICS OF THE ISOLATES OF *C. falcatum*

Sample site 1(SS1)/Isolate No.	Characteristics of colony				
	Colour of colony	Colour of substrate	Margin	Topography	Sporulation
1	White	White	Smooth	Fluffy raised	+
2	White	White	Irregular	Fluffy	+
3	White-grey	White	Smooth	Fluffy raised	+

Note: + indicate the presence of sporulation.

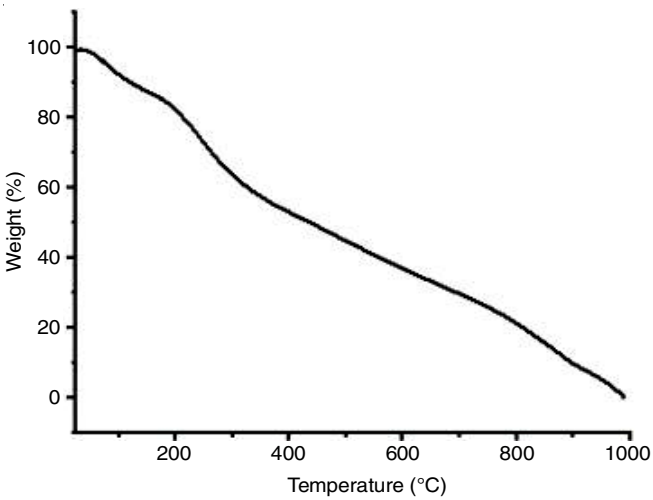

Fig. 5. Thermal analysis of biosynthesized iron oxide nanoparticles

area to volume ratio of the nanoparticles, hence can easily penetrate in to the microbial cell wall/membrane [25].

Photocatalytic activity: Photocatalytic activity of the synthesized nanoparticles was investigated *via* degradation of methylene blue under light exposure by UV-vis measurements at regular interval of times (0, 10, 15, 20, 25 and 30 min, respectively). From the result shown in Fig. 6, a drastic change from the initial time (0 min) down to 0.5 h was observed. This had happened due to the photocatalytic/activity of the synthesized nanoparticles which gave rise to the decolorization of the organic dye from blue to colourless within 0.5 h. Upon exposure to solar, the photons of the sunlight hit the particles

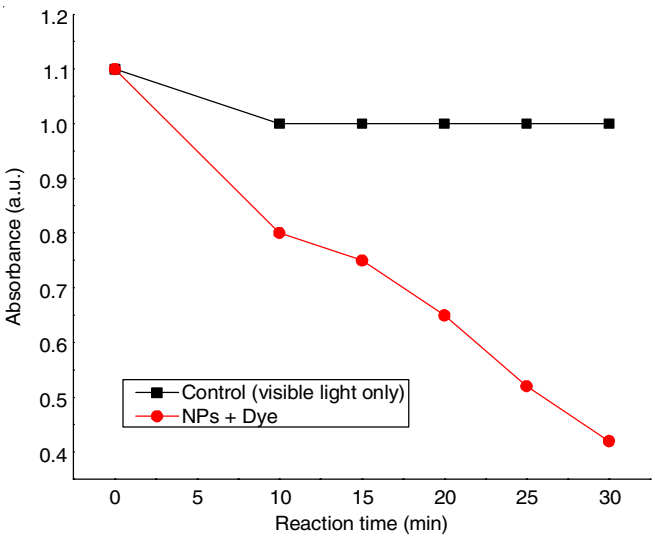

Fig. 6. Photocatalytic activity of biosynthesized iron oxide nanoparticle

that are in the reaction mixture thereby leading to electrons excitation of the nanoparticles surface. The organic dye molecular structure was then breaks down by the anion radicals thereby producing simple molecule and a quick methylene blue dye degradation [26]. The dye degradation obtained in this study was about 81% within a 0.5 h.

The high efficiency degradation might be due to the composition of the biosynthesized nanoparticles as well as the intensity of the visible light. Furthermore, in the mechanism of photocatalytic of the synthesized iron oxide nanoparticles after exposure to sunlight. In nanoparticles, there was an excitation of the electrons in VB toward CB for the same quantity production holes in VB, as such, it create the electron-lone pair production. In addition, separation and migration of charge of the charge carrier that has been produced to the catalyst surface could lead to reaction (redox) with organic dyes. In the hole (h^+) (VB of) high oxidative potential from the catalyst, causes direct oxidation of methylene blue dye to intermediates reactive. Hydroxyl radicals can then be produced following water decomposition. From the other side, the dissolved oxygen molecules as stated earlier reacted with the electrons thereby leading to the production of superoxide anions radical, $O_2^{\bullet-}$, and hydroxyl radical formation $HO_2^{\bullet}$ and eventually with high efficiency of $OH^{\bullet}$ radical [27,32]. Thus, the biosynthesized iron oxide nanoparticles could take part in significant role for the stable and efficient photocatalysis of organic dye degradation in the presence of solar.

Conclusion

The use of clove (*Syzygium aromaticum*) extract for the synthesis of iron oxide nanoparticles was conducted and characterized. In addition, the method was found to be highly ecofriendly, simple and efficient. The synthesized iron oxide nanoparticles have shown a spherical morphology. The dynamic light scattering (DLS) and zeta potential studies have shown a relative stability of the biogenic iron oxide nanoparticles. The activity of the biosynthesized nanoparticles on phytopathogen (*C. falcatum*) revealed the antimicrobial potentiality of the synthesized iron oxide nanoparticles. As a result of bioactive components found in it as well as the small size and large surface area to volume ratio of the biogenic nanoparticles. The photocatalytic activity of the present study can be used for the degradation of an organic methylene blue dye within short time (0.5 h) and also applicable for the treatment of plant pathogenic disease.

Need clear pictures

Write the reason why relative stability.

According to the previous lectures what are the potential mechanisms of Iron oxide nanoparticles against fungal.

I think you need more references

REFERENCES

1. N.M. Noah, *J. Nanomater.*, **2020**, 8855321 (2020); https://doi.org/10.1155/2020/8855321
2. H. Su, S. Li, Y. Jin, Z.Y. Xian, D. Yang, W. Zhou, F. Mangaran, F. Leung, G. Sithamparanathan and K. Kerman, *Adv. Health Care Technol.*, **2017**, 19 (2017); https://doi.org/10.2147/AHCT.S94025
3. M.S. Chavali and M.P. Nikolova, *SN Appl. Sci*., **1**, 607 (2019); https://doi.org/10.1007/s42452-019-0592-3
4. T.C. Dakal, A. Kumar, R.S. Majumdar and V. Yadav, *Front. Microbiol*., **7**, 1831 (2016); https://doi.org/10.3389/fmicb.2016.01831
5. I.X. Yin, J. Zhang, I.S. Zhao, M.L. Mei, Q. Li and C.H. Chu, *Int. J. Nanomed.*, **15**, 2555 (2020); https://doi.org/10.2147/IJN.S246764
6. T. Bruna, F. Maldonado-Bravo, P. Jara and N. Caro, *Int. J. Mol. Sci*., **22**, 7202 (2021); https://doi.org/10.3390/ijms22137202
7. R. Anand and M. Bhagat, *MOJ Biol. Med*., **4**, 19 (2019); https://doi.org/10.15406/mojbm.2019.04.00107
8. H.H. Amin, *Open Agric.*, **5**, 291 (2020); https://doi.org/10.1515/opag-2020-0032
9. K.S. Siddiqi, A. Rahman, Tajuddin and A. Husen, *Nanoscale Res. Lett*., **13**, 141 (2018); https://doi.org/10.1186/s11671-018-2532-3
10. M.G. Demissie, F.K. Sabir, G.D. Edossa and B.A. Gonfa, *J. Chem.*, **2020**, 7459042 (2020); https://doi.org/10.1155/2020/7459042
11. A. Ali, H. Zafar, M. Zia, I. ul Haq, A.R. Phull, J.S. Ali and A. Hussain, *Nanotechnol. Sci. Appl.*, **9**, 49 (2016); https://doi.org/10.2147/NSA.S99986
12. B. Issa, I.M. Obaidat, B.A. Albiss and Y. Haik, *Int. J. Mol. Sci*., **14**, 21266 (2013); https://doi.org/10.3390/ijms141121266
13. K. Hedayati, M. Goodarzi and D. Ghanbari, *J. Nanostruct.*, **7**, 32 (2017); https://doi.org/10.22052/jns.2017.01.004
14. L. Marinescu, D. Ficai, O. Oprea, A. Marin, A. Ficai, E. Andronescu and A.-M. Holban, *J. Nanomater.*, **2020**, 6651207 (2020); https://doi.org/10.1155/2020/6651207
15. S.V. Gopal, R. Mini, V.B. Jothy and I.H. Joe, *Mater. Today Proc.*, **2**, 1051 (2015); https://doi.org/10.1016/j.matpr.2015.06.036
16. A.G. Leonel, H.S. Mansur, A.A.P. Mansur, A. Caires, S.M. Carvalho, K. Krambrock, L.E.F. Outon and J.D. Ardisson, *Int. J. Biol. Macromol.*, **132**, 677 (2019); https://doi.org/10.1016/j.ijbiomac.2019.04.006
17. V. Neveu, J. Perez-Jiménez, F. Vos, V. Crespy, L. du Chaffaut, L. Mennen, C. Knox, R. Eisner, J. Cruz, D. Wishart and A. Scalbert, *Database*, **2010**, bap024 (2010); https://doi.org/10.1093/database/bap024
18. T. Thenmozhi, N. Rasajna, M.N. Rajesh and N.J. Sushma, *J. Nanosci. Technol.*, **5**, 587 (2019); https://doi.org/10.30799/jnst.178.19050103
19. D.F. Cortés-Rojas, C.R.F. de Souza and W.P. Oliveira, *Asian Pac. J. Trop. Biomed.*, **4**, 90 (2014); https://doi.org/10.1016/S2221-1691(14)60215-X
20. B. Kumar, *J. Compos. Sci.*, **5**, 219 (2021); https://doi.org/10.3390/jcs5080219
21. B. Ajtha, Y.A.K. Reddy, Y. Lee, M.N. Kim and C.W. Ahn, *Appl. Organometal. Chem.*, **33**, e4867 (2019); https://doi.org/10.1002/aoc.4867
22. V. Pandey and D.N. Shukla, *Int. J. Agric. Innov. Res.*, **6**, 23191473 (2017).
23. M.K. Mishra and B. Behera, *J. Crop Sci. Biotechnol.*, **12**, 31 (2009); https://doi.org/10.1007/s12892-008-0066-4
24. M.N. Hassan, S. Afghan and F.Y. Hafeez, *BioControl*, **55**, 531 (2010); https://doi.org/10.1007/s10526-010-9268-z
25. S. Parveen, A.H. Wani, M.A. Shah, H.S. Devi, M.Y. Bhat, J.A. Koka, *Microb. Pathog.*, **115**, 287 (2018); https://doi.org/10.1016/j.micpath.2017.12.068
26. K. Roy, C.K. Sarkar and C.K. Gosh, *Dig. J. Nanomater. Biostruct.*, **10**, 107 (2015).
27. S.I. Wanakai, P.G. Kareru, D.S. Makhanu, E.S. Madivoli, E.G. Maina and A.O. Nyabola, *SN Appl. Sci.*, **1**, 1148 (2019); https://doi.org/10.1007/s42452-019-1203-z
28. T.S.J. Kumar, V.R. Akshay, M. Vasundhara and V.A. Muthu, *Colloids Surf. A Physicochem. Eng. Asp.*, **603**, 125241 (2020); https://doi.org/10.1016/j.colsurfa.2020.125241
29. S. Naz, M. Islam, S. Tabassum, N.F. Fernandes, E.J. Carcache de Blanco and M. Zia, *J. Mol. Struct.*, **1185**, 1 (2019); https://doi.org/10.1016/j.molstruc.2019.02.088
30. K. Rajendran, V. Karunagaran, B. Mahanty and S. Sen, *Int. J. Biol. Macromol.*, **74**, 376 (2015); https://doi.org/10.1016/j.ijbiomac.2014.12.028
31. A.U. Mirza, A. Kareem, S.A.A. Nami, M.S. Khan, S. Rehman, S.A. Bhat, A. Mohammad and N. Nishat, *J. Photochem. Photobiol. B*, **185**, 262 (2018); https://doi.org/10.1016/j.jphotobiol.2018.06.009
32. D. Mishra, R. Arora, S. Lahiri, S.S. Amritphale and N. Chandra, *Prot. Met. Phys. Chem. Surf.*, **50**, 628 (2014); https://doi.org/10.1134/S2070205114050128